



Cyclic voltammetry with non-triangular waveforms: Electrochemically irreversible and quasi-reversible systems

Yuki Uchida, Enno Kätelhön, Richard G. Compton^{*}

Department of Chemistry, Physical and Theoretical Chemistry Laboratory, Oxford University, South Parks Road, Oxford OX1 3QZ, United Kingdom

ARTICLE INFO

Keywords:

Cyclic voltammetry
Non-triangular waveforms
Finite difference simulation

ABSTRACT

The voltammetry of electrochemically-irreversible and quasi-reversible reactions are investigated theoretically at a macroelectrode for the case of an applied cosine square-based potential waveform. The results reveal distinct features in the voltammograms which can be exploited to determine the electrochemical transfer coefficient, α , and the standard electrochemical rate constant, k_0 , of a reaction with high sensitivity.

1. Introduction

Cyclic voltammetry is used in electrochemistry for the study of electrode kinetics and the mechanisms of electrode reactions [1–4], providing physical quantities such as the analyte concentrations, diffusion constants, and rate constants through the analysis of voltammograms [5]. A conventional cyclic voltammetry experiment is conducted by applying a potential to the working electrode which is immersed in an electrolyte solution containing the analyte(s) under study and the current response is recorded [1,5,6]. The potential is applied in a linear fashion in the forward and reverse direction with a window large enough to encompass the desired redox reaction known as the triangular potential wave, which is given by the following expression [5]

$$E(t) = \begin{cases} \pm \sigma t + E(t=0) & \text{for } t < t_{1/2} \\ \mp \sigma(t - t_{1/2}) + E(t = t_{1/2}) & \text{for } t \geq t_{1/2} \end{cases} \quad (1)$$

where σ is the scan rate given by the slope of the wave, which has the same value for the forward and reverse sweep but opposite in magnitude, resulting in a discontinuity in its first derivative with respect to time at $t_{1/2}$, the point at which the scan is reversed. Since the capacitive current is proportional to the derivative, this discontinuity results in the discontinuity of the capacitive current. In a real experiment, there are, however, a number of different parasitic capacitances and Ohmic resistances in various parts of the analogue measurement set-up, which compensate for the discontinuity in a complex, partial, and usually unknown fashion.¹ This effect disrupts the voltammetric data and much

complicates the quantitative analysis of experimental results. In a previous paper, we proposed a novel method for cyclic voltammetry using cosine-based potential waveforms, which do not feature any discontinuities in their first derivative and hence avoid the complication [5].

Here, we apply the same cosine-based potential waveform to an electrochemically irreversible and quasi-reversible system to theoretically investigate the voltammetry for varying transfer coefficients [7,8], α , and standard electrochemical rate constants, k_0 . Our analysis reveals that both parameters of an investigated reaction can be determined through the voltammograms resulting from certain cosine-based potential waveforms applied at varying potential offsets with good sensitivity and precision.

2. Theory

In the following, the employed theoretical model is introduced, the method of the cosine-based potential waveform is explained, the dimensionless coordinates used are defined, and the simulation approach is described.

2.1. Theoretical model

We study a one-electron electrochemically irreversible or quasi-reversible reduction reaction of A to B at a planar macroelectrode under diffusion-only conditions, where both species have equal diffusion coefficients:

^{*} Corresponding author.

E-mail address: richard.compton@sjc.ox.ac.uk (R.G. Compton).

¹ A more detailed discussion of the capacitive current in a triangular sweep cyclic voltammogram can for instance be found in the first chapter of the textbook by Bard and Faulkner [3]. The book illustrates the capacitive current for an interface modelled as a series of an ideal Ohmic resistor and an ideal capacitor element. Under experimental conditions as well as in more complex interface models both, the resistance and particularly the capacity of the interface, may however be dependent on the applied potential.

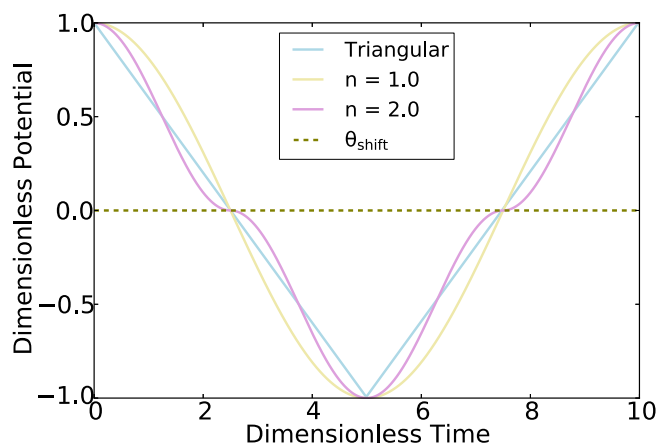


Fig. 1. Triangular, cosine, and cosine squared potential waves centred at 0 with an amplitude of 1. Light blue represents triangular wave, yellow represents cosine function wave with $n = 1$, and light purple represents cosine function wave with $n = 2$. Figure has been adapted from [5]. The dotted line shows the dimensionless potential shift. (For interpretation of the references to color in this figure legend, the reader is referred to the web version of this article.)



When the electrode kinetics are fast compared to the mass transport, the system is termed electrochemically reversible and the concentration of the electroactive species at the electrode surface can be described using the Nernstian equation [1,5,9,10]. The system of interest, on the other hand, is assumed to be irreversible in which the electrode kinetics are slow compared to the mass transport and hence the electrode kinetics described using the Butler-Volmer equation [2,4] drive the reaction:

$$j = k_0 \exp \left[\frac{-\alpha F(E - E_f^0)}{RT} \right] c_{A_0} - k_0 \exp \left[\frac{(1 - \alpha) F(E - E_f^0)}{RT} \right] c_{B_0} \quad (3)$$

where j is the flux of the reactant to the electrode surface, c_{A_0} and c_{B_0} are the concentrations of species A and B at the electrode surface respectively, and k_0 is the standard electrochemical rate constant. This system considers diffusion as the exclusive means of mass transport of the analytes to the electrode surface with no convection and the presence of a sufficiently high concentration of supporting electrolyte is assumed so that migration can be neglected [11–15]. Note, however, that convection needs to be taken into consideration when using long scan duration times [1,3,5,16–18]. The transport of analytes is thus described by the one-dimensional diffusion equation given by Fick's second law [19,20]:

$$\frac{\partial c_j}{\partial t} = D \frac{\partial^2 c_j}{\partial x^2} \quad (4)$$

where j is the species under study and D is its diffusion coefficient. Boundary conditions are established under the assumption that initially only species A is present in the bulk solution [1,19] and prior to applying potential, the concentrations of both A and B are uniform in space [5]:

$$t \leq 0, \quad \text{all } x, \quad c_A = c_A^*, \quad c_B = 0 \quad (5)$$

With increasing t , the values of c_A and c_B change near the electrode surface but no change is observed at the outer boundary surface set sufficiently far from the electrode to give the condition:

$$t > 0, \quad x \rightarrow \infty, \quad c_A = c_A^*, \quad c_B = 0 \quad (6)$$

From conservation of mass, the amount of A consumed at the electrode surface must equal the amount of B produced:

$$t > 0, \quad x = 0, \quad -\frac{\partial c_A}{\partial x} = \frac{\partial c_B}{\partial x} \quad (7)$$

Table 1
Dimensionless parameters [19].

Parameter	Normalization
Concentration	$C_j = \frac{c_j}{c_A^*}$
Diffusion coefficient	$d_j = \frac{D_j}{D_A}$
Spatial coordinate	$X = \frac{x}{\epsilon}$
Time	$\tau = \frac{D_A t}{\epsilon^2}$
Potential	$\theta = \left(\frac{F}{RT} \right) (E - E_f^0)$
Scan rate	$\sigma = \left(\frac{\epsilon^2}{D_A} \right) \left(\frac{F}{RT} \right) \nu$
Current	$J = \frac{i}{\pi \epsilon F D_A c_A^*}$
Rate constant	$K_0 = \frac{k_0 \epsilon}{D}$

assuming $D_A = D_B$, and hence for equal diffusion coefficients the following condition holds true for all space and time.

$$c_A + c_B = c_A^* \quad (8)$$

2.2. Voltammetric scan

As described earlier, the conventional triangular potential wave results in the perturbation of the voltammetric data due to the discontinuity in the capacitive current. However, the complexity of the aforementioned capacitive current can be reduced through the application of a cosine-based function wave, which is given as [5]:

$$E(i) = A \cdot |\cos(2\pi \cdot a \cdot i \Delta t)|^n \cdot \frac{\cos(2\pi \cdot a \cdot i \Delta t)}{|\cos(2\pi \cdot a \cdot i \Delta t)|} + E_{shift} \quad (9)$$

where A is the amplitude of the wave in Volts, a is an auxiliary coefficient defined as $\nu_{avg} \cdot \frac{1}{4A} \cdot 2$ with ϵ representing the radius of the electrode, ν_{avg} is the average scan rate in Volts per second, i is the time step, Δt is the difference between each time step, n is the power of the function, and E_{shift} , defined as $E_{avg} - E_f^0$, is the offset of the wave which is the vital information when analyzing results.

Fig. 1 shows the conventional triangular potential wave and cosine potential waves when $n = 1$ and $n = 2$. As can be seen, the duration time remains constant between the triangular and cosine function potential waves but the instantaneous scan rate at each applied potential differs depending on the wave used for non-linear waveforms [5].

2.3. Dimensionless coordinates

For practicality, all results are presented using a dimensionless unit system. The conversion factors between dimensional and dimensionless units are listed in Table 1. By using these expressions, Eq. (9) can be written in dimensionless form where A is now the amplitude of the dimensionless potential, $a = \frac{\sigma_{avg}}{4A}$ where σ_{avg} is the dimensionless average scan rate, and $\theta_{shift} = \theta_{avg} - \theta_f^0$ for which θ_f^0 is set to equal 0 for simplicity.

2.4. Simulation via finite difference methods

The theoretical model introduced above was simulated via a finite

² We note that in our previous work [5] a was erroneously given as $\frac{\epsilon^2}{D} \cdot \frac{F}{RT} \cdot \nu_{avg} \cdot \frac{1}{4A}$.

$$E_{avg} = \frac{1}{t_{max}} \int_0^{t_{max}} E(t) dt \quad (10)$$

where t_{max} is the maximum scan duration time.[5]

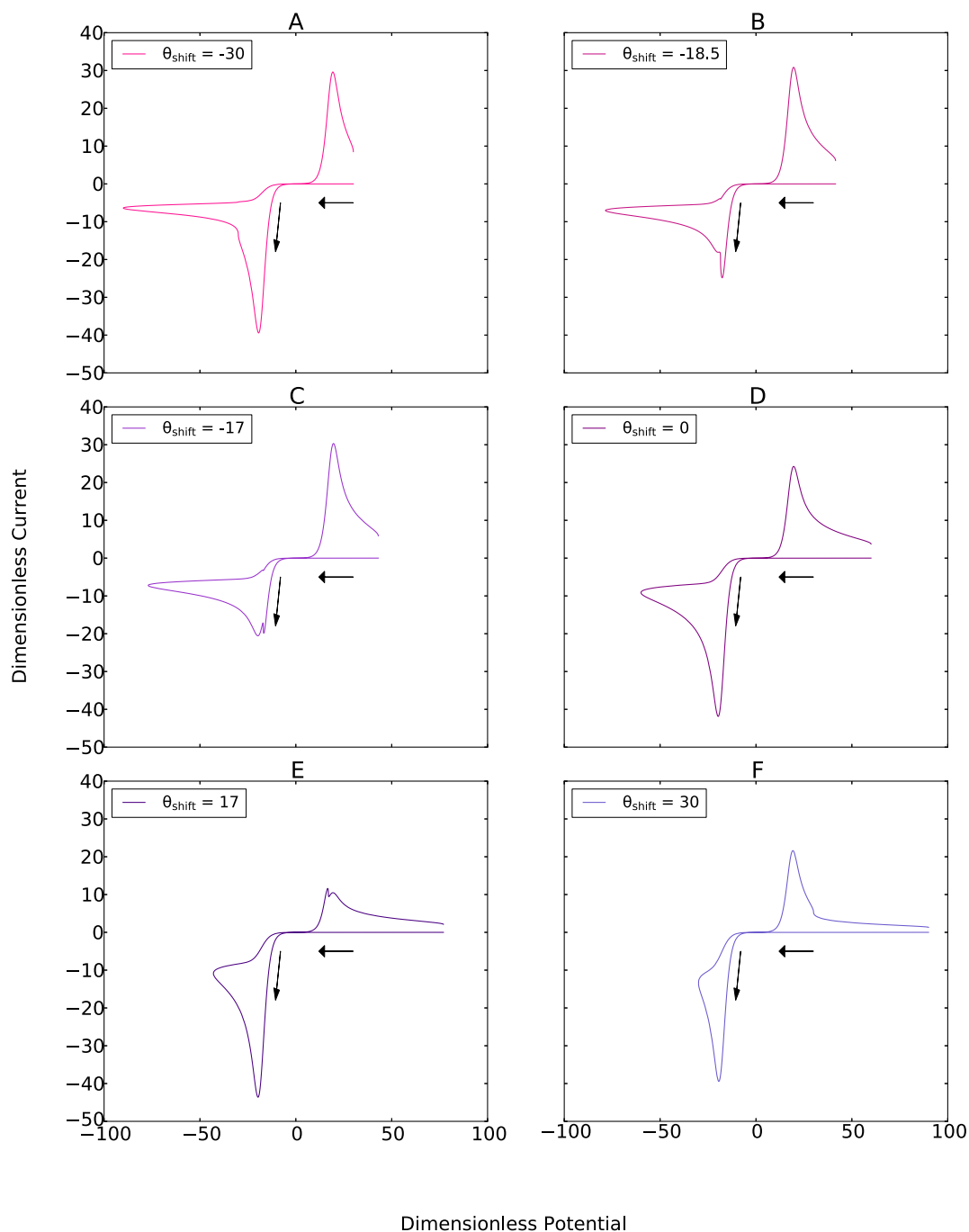


Fig. 2. Voltammograms using a cosine squared potential wave ($n = 2$) with an α of 0.5 and K_0 of 10^{-2} . A represents the voltammogram when $\theta_{\text{shift}} = -30$, B is when $\theta_{\text{shift}} = -18.5$, C is when $\theta_{\text{shift}} = -17$, D is when $\theta_{\text{shift}} = 0$, E is when $\theta_{\text{shift}} = 17$, and F is when $\theta_{\text{shift}} = 30$ in dimensionless coordinates. The arrows show the direction of the sweep.

differences approach by discretizing the dimensionless diffusion equation and using the backward implicit method [5,19,21]. The model was implemented in C++ and plotting was performed in *Python* through the packages *NumPy* and *matplotlib*. Thorough software testing is essential [22] and various convergence tests were run by comparing the peak-to-peak separations, peak heights, peak position with theoretical predictions for triangular potential waveforms, and testing conservation of mass.

3. Results and discussion

In the following, we model the voltammetry of the cosine squared

($n = 2$) potential sweeps for potential windows shifted with respect to the formal potential for different transfer coefficients, α , ranging from 0.4 to 0.6. We focus on the analysis of the results obtained through the cosine squared potential sweeps since the “inflection point” in the potential waveform seen in Fig. 1 at dimensionless times $\frac{1}{4}t_{\text{max}}$ and $\frac{3}{4}t_{\text{max}}$ are seen to be beneficial for the problem addressed. As a paradigm case, we first investigate the system when $\alpha = 0.5$ with varying θ_{shift} values at a scan rate of $\sigma = 10^4$ and $K_0 = 10^{-2}$ where K_0 corresponds to the dimensionless electrochemical rate constant. All analysis were performed on systems with an amplitude of 60 dimensionless units.

Fig. 2 shows the voltammograms obtained using a cosine squared potential wave for which the transfer coefficient is kept at 0.5 and K_0 at

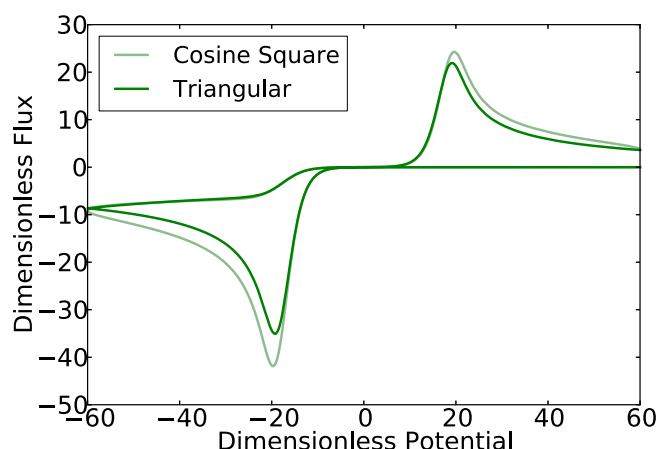


Fig. 3. Voltammogram using a triangular potential wave with an $\alpha = 0.5$, $\sigma = 10^4$, $K_0 = 10^{-2}$ superimposed on Fig. 2D on the same scale.

0.01 for all six voltammograms while the potential window is shifted. Fig. 2A is when $\theta_{\text{shift}} = -30$, Fig. 2B is when $\theta_{\text{shift}} = -18.5$, Fig. 2C is when $\theta_{\text{shift}} = -17$, Fig. 2D is when $\theta_{\text{shift}} = 0$, Fig. 2E is when $\theta_{\text{shift}} = 17$, and Fig. 2F is when $\theta_{\text{shift}} = 30$ in dimensionless coordinates. When the potential shift is significantly negative such as in Fig. 2A, the voltammogram shows one large peak. As the shift becomes less negative, a clear peak split emerges due to the inflection point in the cosine squared wave. The arrows indicate the direction of the sweep and hence the peak that emerges first is labeled as peak 1 and the second one as peak 2 in later analysis. The double peaks become most noticeable at around $\theta_{\text{shift}} = -17$ (Fig. 2C) but when the applied potential wave is symmetric with respect to the formal potential, the voltammogram is similar to the results from a triangular wave shown in Fig. 3. Fig. 3 also shows an amplified version of Fig. 2D. As evident, the two figures show similar features regarding the shape, position of peaks, and their peak heights.

This behavior is explained by the fact that the inflection point in the cosine squared wave occurs in the potential region where no electrode reaction is observed and hence has less effect on the current response. It is clear that the voltammograms change their shapes depending on the θ_{shift} value and consequently the peak heights and peak-to-peak separations will change accordingly.

In addition to the voltammetric response to the potential shift, we also investigated the effect of a varied transfer coefficient. Fig. 4 was plotted using different α values while keeping the θ_{shift} constant. Fig. 4A is the resulting voltammogram when $\alpha = 0.4$, Fig. 4B is when $\alpha = 0.44$, Fig. 4C is when $\alpha = 0.48$, Fig. 4D is when $\alpha = 0.5$, Fig. 4E is when $\alpha = 0.56$, and Fig. 4F is when $\alpha = 0.6$ at the same θ_{shift} value.

Since the double peaks are most prominent at $\theta_{\text{shift}} = -17$ when $\alpha = 0.5$, we chose to use the same potential shift for comparison. From Fig. 4, it is clear that the peak splits occur at different potential shifts for varying α 's. At $\alpha = 0.5$, the two peaks are prominent but as α decreases, one of the peaks diminishes whereas when α increases, the two peaks merge into one. This is because when α is less than 0.5, the double peaks emerge at an θ_{shift} lower than -17 whereas when α is greater than 0.5, the double peaks emerge at an θ_{shift} greater than -17 . These features are clearer when the peak heights are plotted against the potential shift for varying α . Fig. 5 shows the peak heights obtained using various θ_{shift} for the same α shown in Fig. 4. Here, light blue represents the peak height obtained using a triangular potential wave, and light purple (labeled as CosineSquare1) and dark purple (labeled as CosineSquare2) represent peak 1 and peak 2 respectively when $n = 2$ using the cosine function wave.

From Fig. 4, we show that a peak split occurs at a specific θ_{shift} , which is identified through the light purple and dark purple dots in Fig. 5. If we look at the paradigm case when $\alpha = 0.5$, only one peak is

observed in the significantly negative θ_{shift} region which is shown through the perfect overlap of the light and dark purple dots. Near $\theta_{\text{shift}} = -18$ dimensionless potential units, a peak split is observed in which the first peak (represented in light purple) is dominant. However, at $\theta_{\text{shift}} = -17$ the two lines intersect which corresponds to 2C in Fig. 2. Beyond the point of intersection, peak 2 (represented by dark purple) becomes more dominant while peak 1 approaches 0. Examining Fig. 5A, B, and C in Fig. 5, it is clear that the point of intersection happens at a potential shift more negative than -17 when α is less than half, which explains why the first peak is much smaller compared to the second in Fig. 4A, B, and C. When the system is fully irreversible such as that shown in Fig. 4, we can extract interesting information by plotting the minimum peak height of the cosine squared voltammogram extracted from Fig. 5 against α , as shown in Fig. 6.

The dots in Fig. 6 correspond to the minimum peak height using each α value of 0.4, 0.42, 0.44, 0.46, 0.48, 0.5, 0.52, 0.54, 0.56, 0.58, and 0.6 from left to right, and the solid line running through the dots was plotted by performing a linear regression on them. The minimum peak height shows a near-linear dependence on the transfer coefficient, which can be used to interpolate the α value of a redox system under study. For further confirmation of this characteristic feature, identical analysis was performed using a higher rate constant, $K_0 = 0.1$ (also fully-irreversible). The triangles represent the minimum peak heights obtained from a figure similar to Fig. 5 plotted for this new K_0 with all other parameters equal, and the dashed line shows the linear regression performed on the triangular points. The nearly-perfect overlap of the dots and triangles show that the peak heights hardly change with varying rate constants as expected in the fully-irreversible range. This analysis does not require the knowledge of the formal potential since it is only concerned with the minimum peak height and thus the peak heights can be obtained for a range of θ_{shift} until a minimum is observed. Fig. 6 shows that the transfer coefficient can be estimated from the analysis of peak heights for a fully irreversible system. An analysis of the peak-to-peak separation when the back peak is available, on the other hand, can give an estimate of the rate constant and hence the reversibility of the system since these values are sensitive to K_0 , and can also be used to estimate the formal potential as shown below.

Fig. 7 gives the trend of the peak-to-peak separation plotted against θ_{shift} for varying K_0 's with an α of 0.5. Its usefulness arises from the fact that it can be plotted without the pre-knowledge of the formal potential and allows the estimation of K_0 and θ_f^0 . From simple observation it is clear that the peak-to-peak separation values are sensitive to the K_0 of the system and the difference in potential between the two maxima, the point adjacent to the minima, in each plot decreases with increasing K_0 . By comparing the plot of the peak-to-peak separation against θ_{shift} obtained from experimental results to Fig. 7, K_0 for experimental results can be easily obtained. When K_0 is very high, the system approaches full reversibility and the plot of peak-to-peak separation against θ_{shift} looks very similar to that shown in previous work [5]. Since the difference in potential between the two maxima in all of the plots are almost symmetric with respect to $\theta_{\text{shift}} = 0$, which as described earlier, is defined as $\theta_{\text{avg}} - \theta_f^0$, the formal potential can be estimated from the midpoint between the two maxima of each plot. It is, however, important to keep in mind that the shape of the plots given in Fig. 7 change with varying α 's as discussed below and thus K_0 may differ slightly and the formal potential may be under-estimated or over-estimated depending on α .

Fig. 8 shows the peak-to-peak separations plotted against the potential shift values for the same α as in Figs. 4 and 5 for a fully-irreversible system with a K_0 of 0.01. Light blue represents the peak-to-peak separation values of the voltammogram resulting from a triangular potential wave and light purple represents the peak-to-peak separation values when $n = 2$ using the cosine function wave. The peak-to-peak separation of the voltammogram obtained using a triangular potential wave shows a constant value for the varying potential shifts at a certain α . The most interesting features are observed for the results

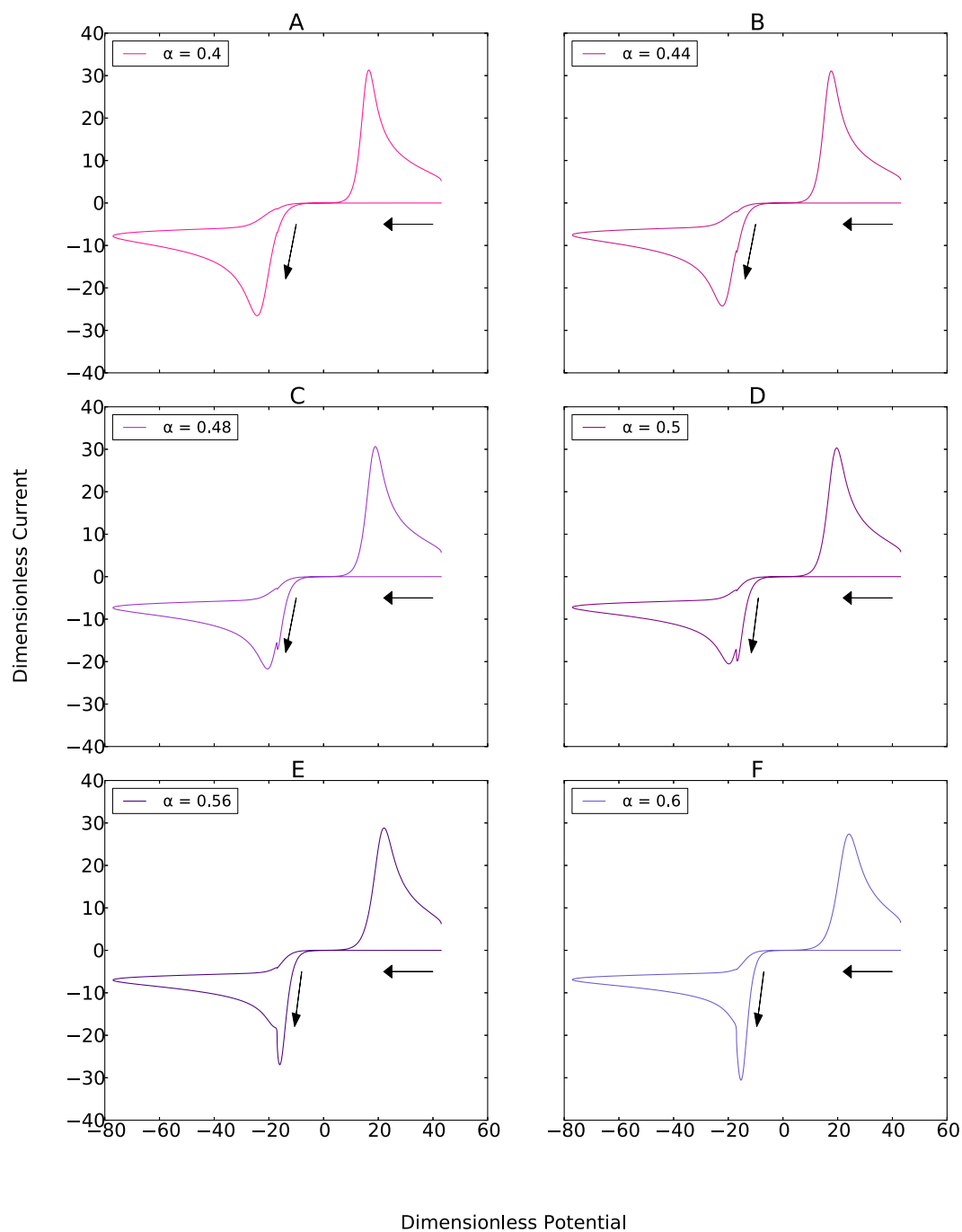


Fig. 4. Voltammograms using a cosine squared potential wave with varying α values. A represents the voltammogram when $\alpha = 0.4$, B is when $\alpha = 0.44$, C is when $\alpha = 0.48$, D is when $\alpha = 0.5$, E is when $\alpha = 0.56$, and F is when $\alpha = 0.6$ at $\theta_{shift} = -17$ dimensionless coordinates and $K_0 = 10^{-2}$. The arrows show the direction of the sweep.

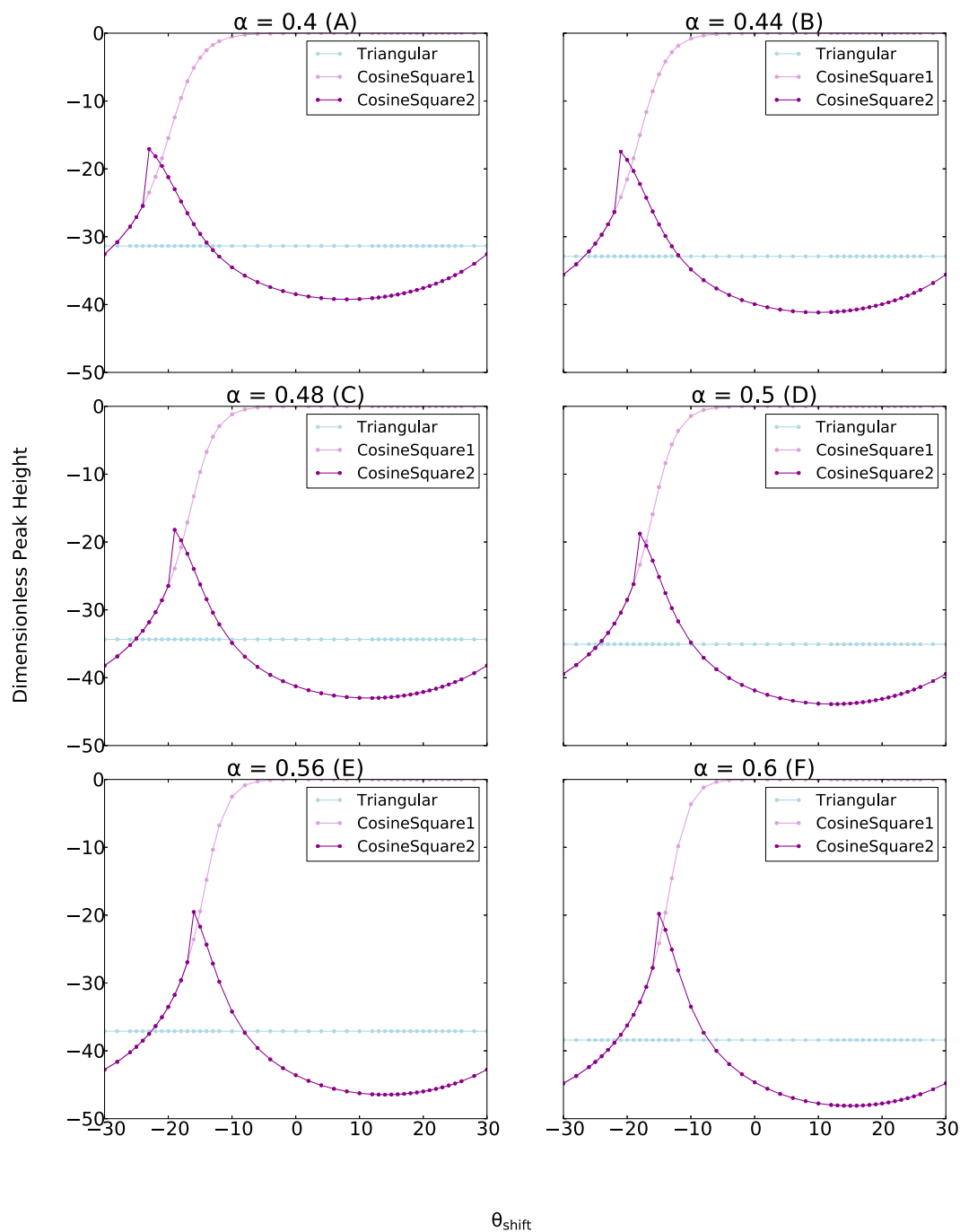


Fig. 5. Peak height against corresponding potential shift for varying α values at a constant K_0 of 10^{-2} . The light blue represents the peak height when using a triangular wave, and light purple (labeled CosineSquare1) and dark purple (labeled CosineSquare2) represent the first peak height (peak 1) and second peak height (peak 2) respectively when $n = 2$ using the cosine function wave with an amplitude of 60 dimensionless units. (For interpretation of the references to color in this figure legend, the reader is referred to the web version of this article.)

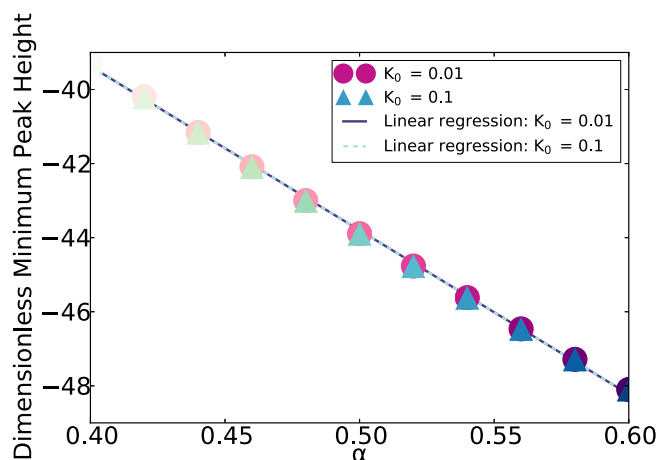


Fig. 6. Minimum peak height obtained through the application of a cosine squared potential wave plotted against α ranging from 0.4 to 0.6 for $K_0 = 10^{-2}$ and $K_0 = 0.1$ with an amplitude of 60 dimensionless units. The dots represent results of $K_0 = 0.01$ and the triangles represent results of $K_0 = 0.1$. The solid line and dashed line were plotted by performing a linear regression on the dots and triangles respectively.

using the cosine function wave when $n = 2$, where there are two regions in which the peak-to-peak separation shows a rapid decrease followed by a sudden increase. Looking at the figures from negative θ_{shift} towards positive θ_{shift} , there is a first minima and first maxima for all of them, and in a fully-irreversible range, if the back peak is available these values can be used for further confirmation of the transfer coefficient.

Fig. 9 shows the trend in the first peak-to-peak separation minima and maxima for various α when $K_0 = 0.01$. The first maxima and minima both show a range of approximately 2 dimensionless potential units, which in dimensional term corresponds to roughly 50 mV (at

25 °C), showing that these values are sensitive to the transfer coefficients when a cosine squared potential wave is applied. The same analysis performed for a system with $K_0 = 0.1$ shows a similar trend and sensitivity as given in Fig. 10. The sensitivity of the first minimum peak-to-peak separation value to the transfer coefficient is further validated by plotting the first minima of the peak-to-peak separation against the potential shift at which it is observed for varying α 's.

As evident from both, Figs. 11 and 12, the first peak-to-peak separation minima are observed at different θ_{shift} values for every α . The above results show that the voltammetric features are highly sensitive to θ_{shift} and hence the α value of a redox couple estimated through the analysis of Fig. 6 can be confirmed by using cosine function waves with $n = 2$ by shifting the window either in the positive or negative direction. It is, however, important to emphasize that the confirmation of α value through peak-to-peak separation can only be done when the back peak is available for an electrochemically fully-irreversible system.

4. Conclusions

We suggest a novel approach to finding the transfer coefficient of a redox system by means of implementing a cosine-based function wave with an exponent of $n = 2$ as the applied potential. The inflection point observed in the potential wave results in a double peak in the voltammogram giving rise to distinct features in the peak height and peak-to-peak separation. It has been established from previous work that cosine function potential waves can reduce the complexity of the capacitive current in experimental data. In addition, the aforementioned features can be exploited as a means to experimentally determine the transfer coefficient of an electrochemically irreversible reaction of interest. Further the peak-to-peak separation analysis with varying potential shifts gives information on the standard electrochemical rate constant of the system under study.

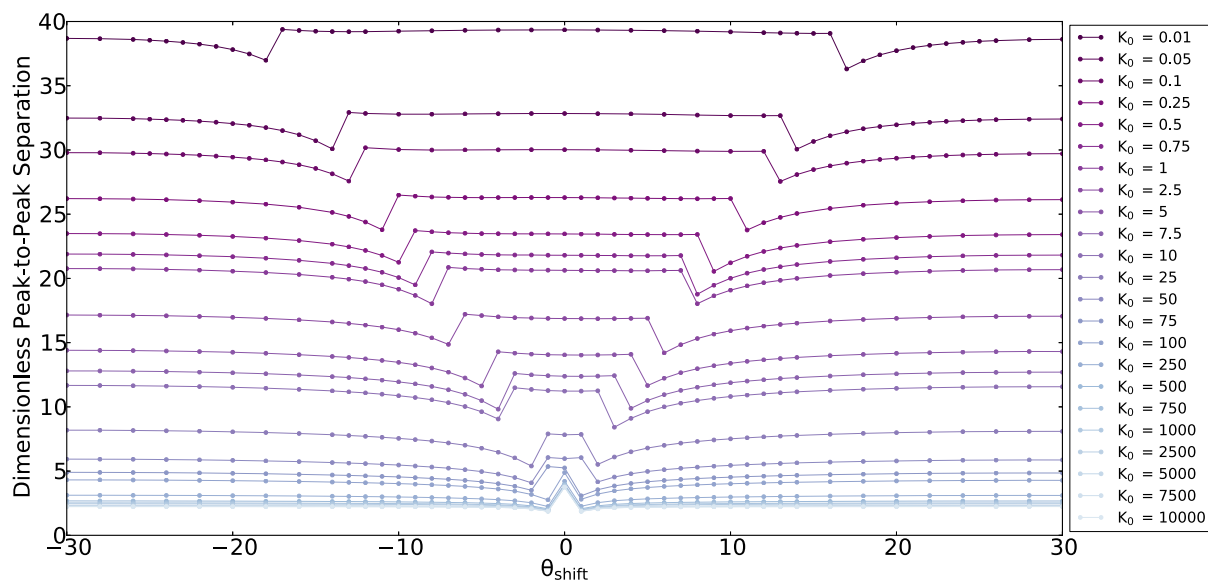


Fig. 7. Peak-to-peak separation against corresponding θ_{shift} values for varying K_0 at $\alpha = 0.5$. The individual K_0 values used are listed in the label with the corresponding colors of the plots.

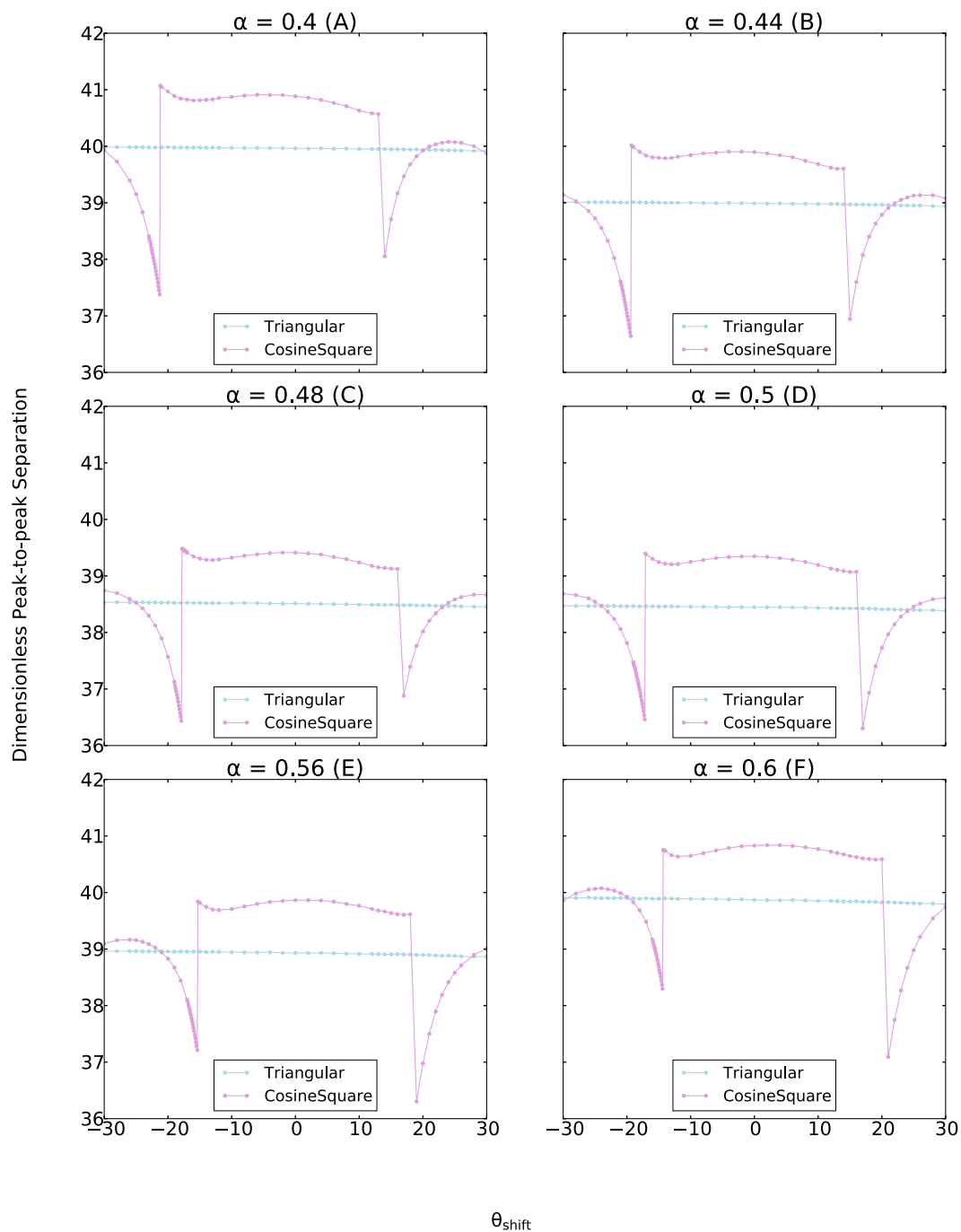


Fig. 8. Peak-to-peak separation against corresponding potential shift with varying α values with K_0 of 0.01. Light blue represents the peak-to-peak separation value obtained using a triangular potential wave and light purple represents the peak-to-peak separation value obtained when $n = 2$ using the cosine function wave. (For interpretation of the references to color in this figure legend, the reader is referred to the web version of this article.)

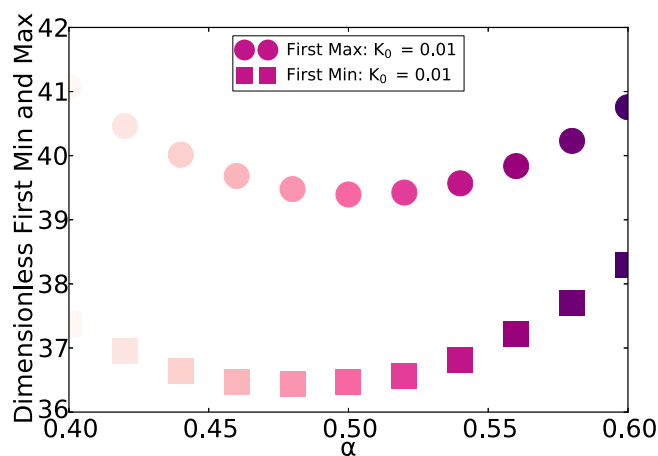


Fig. 9. First minima and maxima peak-to-peak separations against corresponding α values when $n = 2$ using the cosine function wave with K_0 of 0.01.

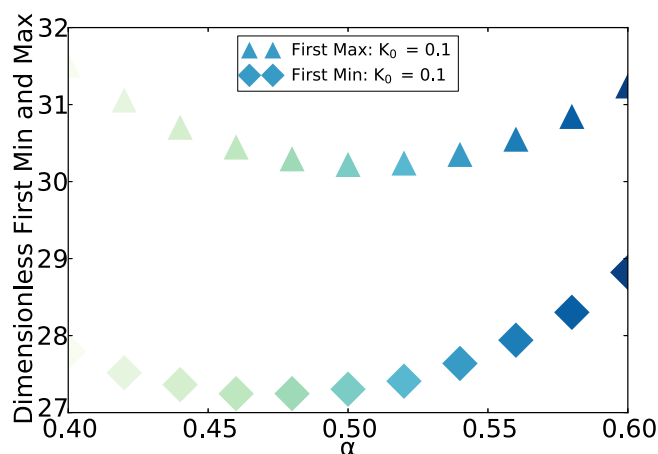


Fig. 10. First minima and maxima peak-to-peak separations against corresponding α values when $n = 2$ using the cosine function wave with K_0 of 0.1.

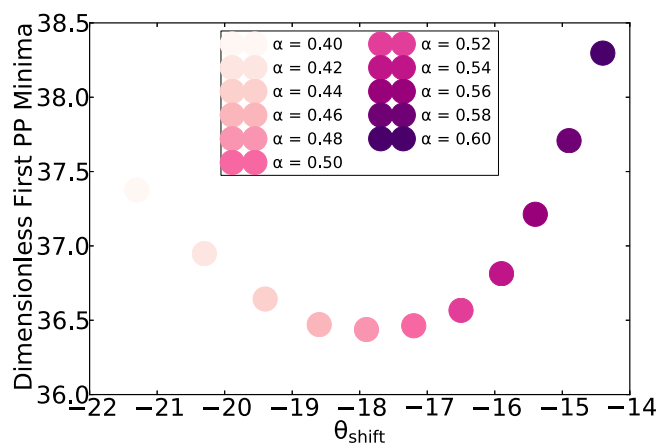


Fig. 11. First minima of peak-to-peak separations against the potential shift value at which they are observed when $n = 2$ using the cosine function wave with K_0 of 0.01.

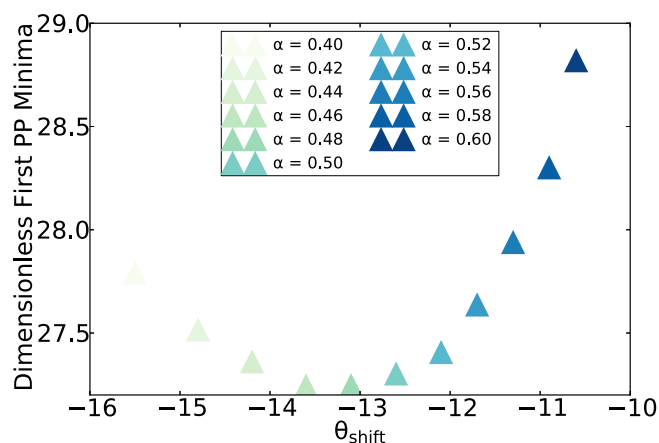


Fig. 12. First minima of peak-to-peak separations against the potential shift value at which they are observed when $n = 2$ using the cosine function wave with K_0 of 0.1.

Acknowledgments

The research leading to these results has received partial funding from the European Research Council under the European Union's Seventh Framework Programme (FP/2007-2013)/ERC Grant Agreement no. [320403].

References

- [1] R.G. Compton, C.E. Banks, *Understanding Voltammetry* (2nd Edition), Imperial College Press, 2010.
- [2] R.S. Nicholson, I. Shain, Theory of stationary electrode polarography. Single scan and cyclic methods applied to reversible, irreversible, and kinetic systems, *Anal. Chem.* 36 (1964) 706–723.
- [3] A.J. Bard, L.R. Faulkner, *Electrochemical Methods: Fundamentals and Applications* (2nd Edition), John Wiley & Sons Inc, 2000.
- [4] T. Gueshi, K. Tokuda, H. Matsuda, Voltammetry at partially covered electrodes: part II. Linear potential sweep and cyclic voltammetry, *J. Electroanal. Chem. Interfacial Electrochem.* 101 (1979) 29–38.
- [5] Y. Uchida, E. Kätelhön, R.G. Compton, Cyclic voltammetry with non-triangular waveforms: electrochemically reversible systems, *J. Electroanal. Chem.* 801 (2017) 381–387.
- [6] P.T. Kissinger, W.R. Heineman, Cyclic voltammetry, *J. Chem. Educ.* 60 (1983) 702.
- [7] R. Guidelli, R.G. Compton, J.M. Feliu, E. Gileadi, J. Lipkowski, W. Schmickler, S. Trasatti, Definition of the Transfer Coefficient in Electrochemistry (IUPAC Recommendations 2014), 86 (2014), pp. 259–262.
- [8] R. Guidelli, R.G. Compton, J.M. Feliu, E. Gileadi, J. Lipkowski, W. Schmickler, S. Trasatti, Defining the Transfer Coefficient in Electrochemistry: An Assessment (IUPAC Technical Report), 86 (2014), pp. 245–258.
- [9] J.C. Helfrick, L.A. Bottomley, Cyclic square wave voltammetry of single and consecutive reversible electron transfer reactions, *Anal. Chem.* 81 (2009) 9041–9047.
- [10] K.B. Oldham, D.J. Gavaghan, A.M. Bond, A full analytic treatment of reversible linear-scan voltammetry with square-wave modulation, *J. Phys. Chem. B* 106 (2002) 152–157.
- [11] J.R. Selman, J. Newman, Free-convection mass transfer with a supporting electrolyte, *J. Electrochem. Soc.* 118 (1971) 1070–1078.
- [12] C. Amatore, A. Oleinick, I. Svir, Theoretical analysis of microscopic Ohmic drop effects on steady-state and transient voltammetry at the disk microelectrode: a quasi-conformal mapping modeling and simulation, *Anal. Chem.* 80 (2008) 7947–7956.
- [13] M. Ciszowska, L. Zeng, E.O. Stejskal, J.G. Osteryoung, Transport of thallium(I) counterion in polyelectrolyte solution determined by voltammetry with microelectrodes and by pulsed-field-gradient, spin-echo NMR, *J. Phys. Chem.* 99 (1995) 11764–11769.
- [14] S. Ching, R. Dudek, E. Tabet, Cyclic voltammetry with ultramicroelectrodes, *J. Chem. Educ.* 71 (1994) 602.
- [15] E.J.F. Dickinson, J.G. Limon-Petersen, N.V. Rees, R.G. Compton, How much supporting electrolyte is required to make a cyclic voltammetry experiment

- quantitatively diffusional? A theoretical and experimental investigation, *J. Phys. Chem. C* 113 (2009) 11157–11171.
- [16] C. Amatore, C. Pebay, L. Thouin, A. Wang, J.-S. Warkocz, Difference between ultramicroelectrodes and microelectrodes: influence of natural convection, *Anal. Chem.* 82 (2010) 6933–6939.
- [17] C.N. Reilley, G.W. Everett, R. Johns, Voltammetry at constant current: experimental evaluation, *Anal. Chem.* 27 (1955) 483–491.
- [18] K. Ngamchuea, S. Eloul, K. Tschulik, R.G. Compton, Advancing from rules of thumb: quantifying the effects of small density changes in mass transport to electrodes. Understanding natural convection, *Anal. Chem.* 87 (2015) 7226–7234.
- [19] R.G. Compton, E. Laborda, K.R. Ward, *Understanding Voltammetry: Simulation of Electrode Processes*, Imperial College Press, 2013.
- [20] J. Crank, *The Mathematics of Diffusion*, Oxford University Press, 1979.
- [21] D. Britz, *Digital Simulation in Electrochemistry*, Springer Berlin Heidelberg, 2005.
- [22] E. Kätelhön, R.G. Compton, Testing and validating electroanalytical simulations, *Analyst* 140 (2015) 2592–2598.